Aerospace Science and Technology 107 (2020) 106284

Contents lists available at ScienceDirect

Aerospace Science and Technology

www.elsevier.com/locate/aescte

On-board implementation and experimental validation of collaborative transportation of loads with multiple UAVs

T. Bacelar [a], J. Madeiras [a], R. Melicio [a,b], C. Cardeira [a,*], P. Oliveira [a]

[a] IDMEC, Instituto Superior Técnico, Universidade de Lisboa, Portugal
[b] ICT, Dep. de Física, Escola de Ciências e Tecnologia, Universidade de Évora, Portugal

ARTICLE INFO

Article history:
Received 10 October 2019
Received in revised form 24 June 2020
Accepted 13 October 2020
Available online 20 October 2020
Communicated by Christian Circi

Keywords:
Multiple unmanned aerial vehicles
Collaborative robotics
On-board navigation and control systems
Air transportation

ABSTRACT

This paper presents a methodology and the experimental validation for collaborative load transportation using two UAVs (Unmanned Aerial Vehicles). The state variables are estimated, based on measurements from motion sensors installed on-board. Control and estimation solutions were required to ensure the stability of the system, while guaranteeing null steady-state position and estimation errors. The vertical velocity is also estimated since there is no sensor on-board the UAVs capable of providing this measure directly. The relative position between the UAVs is estimated using only on-board sensors and images acquired by the UAV front camera. The controllers and estimators resort to linear and optimal control techniques, as the Linear Quadratic Regulators and Kalman filters. The proposed control system is validated both in simulation and experimentally, resorting to a commercially available quadrotor equipped with an Inertial Measurement Unit, an ultrasound height sensor, vertical and frontal cameras.

1. Introduction

In the last decades, the interest in Unmanned Aerial Vehicles (UAV) has increased. The spectrum was so large that it became necessary to provide a classification and taxonomy for drones. Drones are flying robots which include unmanned air vehicles (UAVs) that fly thousands of kilometers and small drones that fly in confined spaces [1].

For this study, according to [1] the air vehicle used is a MAV (Micro or Miniature Air Vehicle) rotary wing quadrotor, VTOL (Vertical Take Off and Landing) and LASE (Low Altitude, Short-Endurance).

The development and wide commercialization of these types of vehicles turned their use very popular. They can operate in highly constrained environments with multiple hostiles obstacles and impossible to reach by humans. For these reasons, they became very useful for a wide range of civil and military applications, such as environment monitoring, surveillance, search, and rescue missions or transportation of cargo. One of the major limitations on the available models is in terms of payload carrying capacity and range, being required the cooperation of several of these vehicles for several applications.

The problem of load transportation has been addressed in recent works. In [2] the problem of transport of a suspended load by a multirotor aircraft is addressed. In [3][4] the cooperation of multiple UAVs is used for load transportation. In [5] collaborative load transportation using multiple UAVs is presented. Load transportation has also been done effectively in [6] with experimental results. In [7] cooperative load transport force control is addressed. However, most of these works, besides [6] do not involve experimental validation or play with a single UAV. The drone autonomy and battery sizing are addressed in [8].

The manipulation of a towed cable system resorting to an aerial vehicle has been studied in [9]. A control method for the transportation of tethered known loads with a single quadrotor is proposed in [10], resorting to a Mixed Integer Quadratic Program focusing on aggressive maneuvering. Methods to tackle applications where the load is unknown are proposed, both for the estimation and the control of the height of a single quadrotor in [11]. Methods for cooperative manipulation and transportation using multiple aerial vehicles based on quasi-static models are proposed in [12], focusing on the position and orientation control of a payload with six degrees of freedom. The same problem is addressed in [13], studying the dynamics of cooperative manipulation resorting to a complete dynamical model for the cases when the payload is considered to be a three-dimensional rigid body.

In this paper, a method for collaborative load transportation is proposed. It is assumed that the length of the load is greater than

* Corresponding author.
E-mail address: carlos.cardeira@tecnico.ulisboa.pt (C. Cardeira).

https://doi.org/10.1016/j.ast.2020.106284
1270-9638/

the distance between both UAVs as shown in Fig. 2, thus a configuration is envisioned where longitudinal forces are small, and thus will be neglected in the modeling phase and later rejected by the control system. Moreover, the air flow cross disturbance can also be neglected due to the above mentioned geometry.

A position control loop using LQR (Linear Quadratic Regulator) is proposed for the rear UAV, and for estimation a linear Kalman filter is considered. The motion sensors used are a gyroscope, a magnetometer, an ultrasound sensor and a downward pointing camera for optical flow computation proposes, all usually available on-board a UAV. The on-board Inertial Measurement Unit (IMU) allows the measurement and estimation of the height, attitude angles, accelerations, angular, and ground velocities.

Comparing with existing works, in [2] the problem of transport of a suspended load by a multirotor aircraft is addressed, however without cooperation between robots. [3] and [5] present a relatively similar approach to our work, but lacking experimental results. Comparing to [4] also a non collaborative approach is proposed with the same controller to all vehicles. In [6], load transportation using helicopters with experimental results, is presented, but the paper is mainly focused on the system integration of multiple sensors and networks lacking details about the estimation and control strategies. [7] presents a study of cooperative transportation using aerial manipulators, the problem is very interesting but the paper lacks experimental validation. In [9] differential flatness is exploited for the control of one UAV with a towed load, where the generalization to multiple vehicles is not immediate, nor the collaborative approach pursued in the present work. [10] presents effective load transportation with experimental validation resorting however to a single quadrotor. [11] presents load transportation with load mass estimation, however involving no cooperation among robots. In [12][13] solutions for the cooperative manipulation and transportation of loads with aerial robots are proposed. The planning and control are solved for all vehicles thus departing from the collaborative approach, focus of the present work.

The main contribution of this work is an experimental validation of a control and navigation architecture for collaborative load transportation using UAVs.

This paper is organized as follows: the problem addressed in this paper is described in Section 2. The physical model considered is presented in Section 3. The system dynamics is presented in Section 4. The solution for the control problem is proposed in Section 5, and the solution for estimation is presented in Section 6. In Section 7 experimental results are presented and analyzed. Finally, some concluding remarks are presented in Section 8.

2. Problem statement

For control systems design regarding the collaborative transportation of loads with two UAVs, the controllability property plays a crucial role, alongside the observability property which measures how well systems internal states can be inferred from knowledge of its external outputs. The controllability and observability of a system are mathematical duals. A deeper survey can be found in [14]. For the envisioned solution both properties must be verified. The main goal is to control the UAVs 3D inertial position and orientation with respect to a reference North-East-Down (NED) frame. The two quadrotors to be considered are denoted as the front (F) and rear (R) UAV, which configuration is presented in Fig. 2.

Given the difficulties proving the system controllability and observability when considering the two UAVs as an ensemble with one common state space, a different approach is exploited. In this approach, the following project approach is considered:

- The front UAV is piloted by an operator;
- The relative position and orientation between both UAVs is controlled by the rear UAV, using only on-board sensors;
- The load is rigid.

Regarding the control of the front UAV position and orientation, externally to the rear UAV, a control system for the front UAV was designed. The front UAV will be able to follow the operator references, and therefore stably follows the trajectory autonomously. The control systems were designed resorting to optimal control techniques, namely, LQRs, which requires full state feedback. To reduce the noise impact present in the system measurements, and to ensure the full state feedback, discrete linear Kalman Filters are designed.

The relative position between both UAVs is the primary state to control since the system's stability relies on this. Poor control of the relative position may lead to undesirable oscillations and twisting forces which can turn the system unstable resulting in the crash of both UAVs. The rear UAVs frontal camera is used to estimate the relative position, velocity and orientation with respect to the rear UAV body-fixed frame. The relative velocity can be computed resorting to optical flow techniques or resorting to a complementary filter upon the relative position estimation.

Then, concerning the estimation of the relative velocities upon the position measurements, will be designed and implemented complementary filters.

3. Physical model

The physical model is obtained relative to the NED inertial frame, expressing the rigid body dynamics of the quadrotor in the body-fixed frame. A more detailed description of the quadrotor physical model without a load can be found in [15]. In order to distinguish both UAVs, index subscripts $_R$ and $_F$ are used to denote the rear and front UAV, respectively. Let $\boldsymbol{X_N}, \boldsymbol{Y_E}, \boldsymbol{Z_D}$ be the NED inertial frame major axis, $\boldsymbol{X_R}, \boldsymbol{Y_R}, \boldsymbol{Z_R}$ be the Rear UAV NED frame major axis, $\boldsymbol{X_F}, \boldsymbol{Y_F}, \boldsymbol{Z_F}$ be the Front UAV NED frame major axis, $\boldsymbol{v} = (u, v, w)^T$ represent the linear velocity vector in the East-North-Up (ENU) inertial frame, $\boldsymbol{\eta} = (\phi, \theta, \psi)^T$ denote the orientation vector of the body-fixed frame with respect to the inertial frame in terms of Euler angles, and the body-axis angular rate vector be described by $\boldsymbol{\Omega} = (p, q, r)^T$.

4. System dynamics

The mathematical derivation of the non-linear model of the system in this work follows [16,17], resorting to the Lagrange-d'Alembert's principle. However, instead of computing the inertial position of the UAVs upon the position of the payload, the system dynamics are derived expressing the position of the payload in a function of the UAVs position, and taking into consideration the same assumptions.

4.1. Euler-Lagrange equations

Consider n UAVs connected to a payload via mass-less links modeled as a rigid body as depicted in Fig. 3. This figure is similar to Fig. 2 but generalized to n UAVs.

The variables regarding the payload are represented by the index subscript 0, and the variables related to the ith UAV are denoted by the index subscript i, which is assumed to be an element of the set $\mathcal{I} = \{1, \cdots, n\}$. The dynamical model is derived by choosing a NED inertial frame $\{\vec{\boldsymbol{e}}_1, \vec{\boldsymbol{e}}_2, \vec{\boldsymbol{e}}_3\}$ and body-fixed frames $\{\vec{\boldsymbol{b}}_{j1}, \vec{\boldsymbol{b}}_{j2}, \vec{\boldsymbol{b}}_{j3}\}$ for $0 \leq j \leq n$.

For the inertial frame, the third axis $\vec{\boldsymbol{e}}_3$ points downward along the gravity vector, the other axis is chosen in order to form an orthonormal frame. The origin of the jth body-fixed frame is placed

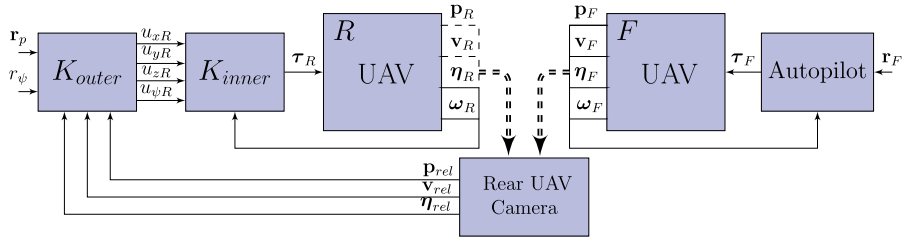

Fig. 1. Collaborative UAVs: control system architecture.

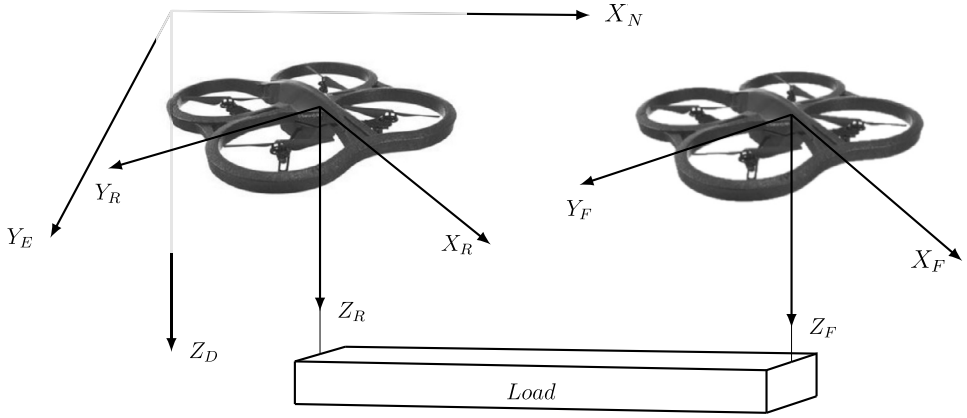

Fig. 2. Rear and front UAV configuration.

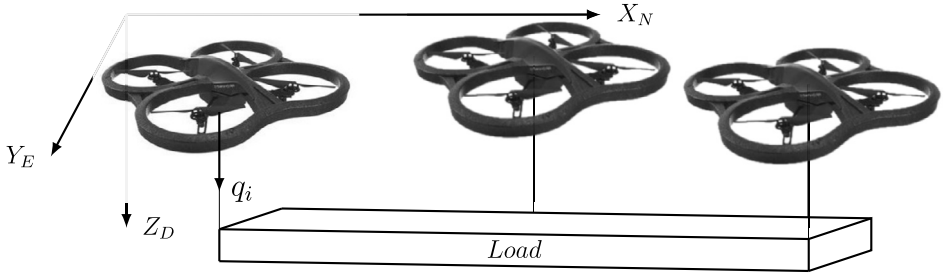

Fig. 3. System configuration for n UAVs.

at the center of mass of the UAV for $1 \leq j \leq n$. The third body-fixed axis $\vec{\boldsymbol{b}}_{j3}$ is normal to the plane defined by the center of the UAVs rotors, and it points downward.

Let $\boldsymbol{x}_i \in \mathbb{R}^3$ be the position of the center of mass of the ith UAV with respect to the inertial frame. The attitude of the ith UAV is defined by $\boldsymbol{R}_i \in \mathrm{SO}(3)$, which represents the rotation matrix that rotates the ith body-fixed frame into the NED inertial frame. The special orthogonal group is given by $\mathrm{SO}(3) = \{\boldsymbol{R} \in \mathbb{R}^{3\times 3} \mid \boldsymbol{R}^T\boldsymbol{R} = \boldsymbol{R}\boldsymbol{R}^T = \mathbf{I},\ det(\boldsymbol{R}) = 1\}$. The mass and the inertia matrix of the ith UAV are defined as $m_i \in \mathbb{R}$ and $\boldsymbol{J}_i \in \mathbb{R}^{3\times 3}$, respectively. The ith UAV generates a total thrust $-f_i\boldsymbol{R}_i\vec{\boldsymbol{e}}_3$ with respect to the inertial frame, where $f_i \in \mathbb{R}$ is the total thrust magnitude, and $\vec{\boldsymbol{e}}_3 = [0 \quad 0 \quad 1]^T \in \mathbb{R}^3$ defined with respect to the inertial frame. The ith UAV also generates a moment $\boldsymbol{\tau}_i \in \mathbb{R}^3$ with respect to its body-fixed frame. Therefore, the control input of this system corresponds to $\{f_i, \boldsymbol{\tau}_i\}_{1\leq i\leq n}$.

The inertial position vector of the center of mass of the payload is defined as $\boldsymbol{x}_0 \in \mathbb{R}^3$, and its attitude is given by $\boldsymbol{R}_0 \in \mathrm{SO}(3)$. The mass and the inertia matrix of the payload are denoted by $m_0 \in \mathbb{R}$ and $\boldsymbol{J}_0 \in \mathbb{R}^{3\times 3}$, respectively. The point on the payload where the ith link is attached is denoted by $\boldsymbol{\rho}_i \in \mathbb{R}^3$, and it is represented with respect to the 0th body-fixed frame. The other end of the link is attached to the center of mass of the ith UAV. The direction of the link is represented from the center of mass of the ith UAV toward the payload is defined by the unit-vector $\boldsymbol{q}_i \in \mathrm{S}^2$, where $\mathrm{S}^2 = \{\boldsymbol{q} \in \mathbb{R}^3 \mid \|\boldsymbol{q}\| = 1\}$. The length of the ith link is defined as $l_i \in \mathbb{R}$. Since the links are assumed to be rigid, the inertial position vector of the center of mass of the payload is given by:

$$\boldsymbol{x}_0 = \boldsymbol{x}_i - \boldsymbol{R}_0\boldsymbol{\rho}_i + l_i\boldsymbol{q}_i \tag{1}$$

The standard dot product is denoted by $\boldsymbol{a}\cdot\boldsymbol{b} = \boldsymbol{a}^T\boldsymbol{b}$ for all $\boldsymbol{a}, \boldsymbol{b} \in \mathbb{R}^3$. The hat map $\widehat{\cdot}: \mathbb{R}^3 \longrightarrow \mathrm{SO}(3)$ is defined by the condition that $\widehat{\boldsymbol{a}}\boldsymbol{b} = \boldsymbol{a}\times\boldsymbol{b}$ for all $\boldsymbol{a}, \boldsymbol{b} \in \mathbb{R}^3$.

Since the inertial position of the mass center of the payload is given by (1), through the computation of its time derivative the linear velocity of the payload is given by:

$$\dot{\boldsymbol{x}}_0 = \dot{\boldsymbol{x}}_i - \dot{\boldsymbol{R}}\boldsymbol{\rho}_i + l_i\dot{\boldsymbol{q}}_i \tag{2}$$

4.2. Kinematic equations

For the UAVs, links and payload the kinematics equations are given by:

$$\dot{\boldsymbol{q}}_i = \boldsymbol{\omega}_i \times \boldsymbol{q}_i = \widehat{\boldsymbol{\omega}}_i\boldsymbol{q}_i \tag{3}$$

$$\dot{\boldsymbol{R}}_0 = \boldsymbol{R}_0\widehat{\boldsymbol{\Omega}}_0, \quad \dot{\boldsymbol{R}}_i = \boldsymbol{R}_i\widehat{\boldsymbol{\Omega}}_i \tag{4}$$

where $\boldsymbol{\omega}_i \in \mathbb{R}^3$ is the angular velocity of the ith link satisfying the condition that $\boldsymbol{q}_i \cdot \boldsymbol{\omega}_i = \mathbf{0}$. $\boldsymbol{\Omega}_i$ and $\boldsymbol{\Omega}_0 \in \mathbb{R}^3$ are the angular velocities of the ith UAV and the payload expressed with respect to its body-fixed frame, respectively.

4.2.1. Kinetic and potential energies

The kinetic energy of the system is composed of the translational kinetic energy and the rotational kinetic energy of the payload and UAVs, is given by:

$$\mathcal{T} = \frac{1}{2} m_0 \left\| \dot{\boldsymbol{x}}_0 \right\|^2 + \frac{1}{2} \boldsymbol{J}_0 \boldsymbol{\Omega}_0 \cdot \boldsymbol{\Omega}_0 + \sum_{i=1}^{n} \frac{1}{2} m_i \left\| \dot{\boldsymbol{x}}_i \right\|^2 + \frac{1}{2} \boldsymbol{J}_i \boldsymbol{\Omega}_i \cdot \boldsymbol{\Omega}_i \tag{5}$$

The gravitational potential energy of the system is given by:

$$\mathcal{U} = -m_0 g \boldsymbol{e}_3 \cdot \boldsymbol{x}_0 - \sum_{i=1}^{n} m_i g \boldsymbol{e}_3 \cdot \boldsymbol{x}_i \tag{6}$$

Based on the Lagrange-d'Alembert principle, after tedious derivations, the Euler-Lagrange equations of motion can be expressed by:

$$\begin{aligned} \left[m_i \mathbf{I} + \boldsymbol{q}_i \boldsymbol{q}_i^T m_0 \right] (\ddot{\boldsymbol{x}}_i - g \boldsymbol{e}_3) + m_0 \boldsymbol{q}_i \boldsymbol{q}_i^T \boldsymbol{R}_0 \widehat{\boldsymbol{\rho}}_i \dot{\boldsymbol{\Omega}}_0 = m_0 l_i \| \boldsymbol{\omega}_i \|^2 \boldsymbol{q}_i \\ + m_0 \boldsymbol{q}_i \boldsymbol{q}_i^T \boldsymbol{R}_0 \widehat{\boldsymbol{\Omega}}_0^2 \boldsymbol{\rho}_i + \boldsymbol{u}_i \end{aligned} \tag{7}$$

$$\boldsymbol{J}_i \dot{\boldsymbol{\Omega}}_i + \boldsymbol{\Omega}_i \times \boldsymbol{J}_i \boldsymbol{\Omega}_i = \boldsymbol{\tau}_i \tag{8}$$

$$\begin{aligned} &\left[\boldsymbol{J}_0 - m_0 \widehat{\boldsymbol{\rho}}_i \boldsymbol{R}_0^T \boldsymbol{q}_i \boldsymbol{q}_i^T \boldsymbol{R}_0 \widehat{\boldsymbol{\rho}}_i \right] \dot{\boldsymbol{\Omega}}_0 \\ &\quad - m_0 \widehat{\boldsymbol{\rho}}_i \boldsymbol{R}_0^T \boldsymbol{q}_i \boldsymbol{q}_i^T (\ddot{\boldsymbol{x}}_i - g \boldsymbol{e}_3) + \widehat{\boldsymbol{\Omega}}_0 \boldsymbol{J}_0 \boldsymbol{\Omega}_0 \\ &\quad = -m_0 \widehat{\boldsymbol{\rho}}_i \boldsymbol{R}_0^T (l_i \| \boldsymbol{\omega}_i \|^2 \boldsymbol{q}_i + \boldsymbol{q}_i \boldsymbol{q}_i^T \boldsymbol{R}_0 \widehat{\boldsymbol{\Omega}}_0^2 \boldsymbol{\rho}_i) \end{aligned} \tag{9}$$

$$m_0 l_i \dot{\boldsymbol{\omega}}_i = m_0 (-\widehat{\boldsymbol{q}}_i \ddot{\boldsymbol{x}}_i + \widehat{\boldsymbol{q}}_i \boldsymbol{R}_0 \widehat{\boldsymbol{\Omega}}_0 \boldsymbol{\rho}_i - \widehat{\boldsymbol{q}}_i \boldsymbol{R}_0 \widehat{\boldsymbol{\rho}}_i \dot{\boldsymbol{\Omega}}_0 + g \widehat{\boldsymbol{q}}_i \boldsymbol{e}_3) \tag{10}$$

The influence of the Coriolis effects and the provided angular moments are given by:

$$m \dot{\boldsymbol{v}} = m \boldsymbol{g} + \boldsymbol{R}_{\mathcal{B}}^{\mathcal{I}} \mathbf{F}^{\mathcal{B}} - \boldsymbol{v} \times \boldsymbol{\omega} \tag{11}$$

where $\boldsymbol{g} = (0, 0, g)^T$ is the gravity vector with respect to the inertial frame, m accounts for the total mass (rear UAV mass plus uncompensated load mass), g is the gravitational acceleration, $\boldsymbol{R}_{\mathcal{B}}^{\mathcal{I}}$ is the rotation matrix responsible for rotate the UAV body-fixed frame into the NED inertial frame is presented in (12). $\mathbf{F}^{\mathcal{B}}$ corresponds to the total force applied in the UAV in terms of a vector with respect to the body-fixed frame presented in (13). Here $\mathbf{f}^{\mathcal{B}}$ is the actuation force vector, $\boldsymbol{g}_{\mathcal{I}}^{\mathcal{B}}$ is the rotation matrix that rotates the NED inertial frame into the body-fixed frame, and $\boldsymbol{t}$ is the tension force applied to the UAV which is assumed to be approximately null.

$$\boldsymbol{R}_{\mathcal{B}}^{\mathcal{I}}(\boldsymbol{\eta}) = \begin{bmatrix} c\psi c\theta & -c\theta s\psi & s\theta \\ c\phi s\psi - c\psi s\theta s\psi & c\psi c\phi + s\psi s\theta s\phi & c\theta s\phi \\ -s\psi s\phi - c\psi c\phi s\theta & c\theta s\psi s\theta - c\psi s\phi & c\theta c\phi \end{bmatrix} \tag{12}$$

$$\mathbf{F}^{\mathcal{B}} = \mathbf{f}^{\mathcal{B}} + \boldsymbol{R}_{\mathcal{I}}^{\mathcal{B}} (\boldsymbol{v} \times \boldsymbol{\omega}) + \boldsymbol{t} \tag{13}$$

Replacing (13) in (11):

$$m \dot{\boldsymbol{v}} = m \boldsymbol{g} + \mathbf{f}^{\mathcal{I}} \tag{14}$$

where $\mathbf{f}^{\mathcal{I}} = \mathbf{R}_{\mathcal{B}}^{\mathcal{I}} \mathbf{f}^{\mathcal{B}}$.

The angular behavior which takes into consideration Coriolis effects influence is given by:

$$\boldsymbol{J} \dot{\boldsymbol{\Omega}} = -\boldsymbol{\Omega} \times \boldsymbol{J} \boldsymbol{\Omega} + \boldsymbol{\tau} \tag{15}$$

where $\boldsymbol{J}$ is the inertia matrix and $\boldsymbol{\tau}$ is the torque vector that results from a combination of differences between the thrust forces generated by each of the four rotors.

5. Control

In this Section the system design is detailed. First, the LQR is introduced followed by the controllers design for both UAVs.

5.1. LQR

Consider the following linear time-invariant (LTI) dynamical system presented in (16). Vector $\mathbf{x}$ is the $n \times 1$ state vector and vector $\mathbf{u}$ is the $m \times 1$ control input. The control input is defined to be the state feedbacks as shown in (17).

$$\dot{\mathbf{x}} = \mathbf{A}\mathbf{x} + \mathbf{B}\mathbf{u} \tag{16}$$

$$\mathbf{u} = -\mathbf{K}\mathbf{x} \tag{17}$$

$$J = \int_0^{\infty} (\mathbf{x}^T \mathbf{Q} \mathbf{x} + \mathbf{u}^T \mathbf{R} \mathbf{u}) dt \tag{18}$$

The state feedback control gain matrix that minimizes the quadratic cost function is denoted as $\mathbf{K}$, as solved by Kalman in [18], presented in (18). In cost function J, the matrices $\mathbf{Q}$ and $\mathbf{R}$ determine the relative importance of the errors in the states or in the control action, respectively. In (18) $\mathbf{Q}$ and $\mathbf{R}$ matrices are defined with units such that the cost function has an energetic interpretation. The values used on these matrices result from a trial and error procedure during real time (or simulated) tests with the vehicles such that the dynamic performances (settling time and tracking errors) reach a good compromise for the users. The control vector $\mathbf{u}(t)$ is assumed to be unconstrained. The infinite time quadratic optimal control problem relies on the minimization of the cost function J. The optimal gain matrix for the infinite time quadratic optimal control problem is linear and is given in (19). The matrix $\boldsymbol{P}$ in (19) must satisfy the algebraic Riccati equation presented in (20).

$$\mathbf{K} = \mathbf{R}^{-1} \mathbf{B}^T \boldsymbol{P} \tag{19}$$

$$\mathbf{A}^T \boldsymbol{P} + \boldsymbol{P}\mathbf{A} - \boldsymbol{P}\mathbf{B}\mathbf{R}^{-1}\mathbf{B}^T \boldsymbol{P} + \mathbf{Q} = 0 \tag{20}$$

The optimal state feedback control gain matrix $\mathbf{K}$ is given by substituting the matrix $\boldsymbol{P}$ obtained by solving the (20) into (19).

5.2. Controllers design

This subsection presents the position and orientation control design for both UAVs. The position control is responsible for maintain the UAV over a desired position.

The position controller for both UAVs is designed and implemented of over an internal attitude control. Since this attitude inner loop is assumed to be significantly faster than the outer loop, the system's planar motion can be interpreted as a dominantly second-order system.

The UAVs are controlled by giving the following set of inputs:

- u_x front/back bending angle, assuming negative values bending forward and zero on the horizontal plane;
- u_y left/right bending angle, assuming negative values bending leftward;
- u_z vertical speed;
- u_ψ angular speed around the yaw axis.

5.2.1. Front UAV

For the front UAV, the objective is the design of an autopilot external control loop by giving as input the desired inertial position and orientation values, denoted as $\mathbf{r}_F$, in order to maintain the UAV in the desired position. This autopilot is responsible for translating the input references into thrust forces to be generated by each rotor, resorting the inertial position, body-fixed frame velocities, Euler angles and rates, measured using sensors installed on-board.

5.2.2. Rear UAV

The control system for the rear UAV could also be a commercially available autopilot, however controllability would be compromised. Thus, for the rear UAV, the objective is the design of an external control loop by giving the desired relative position and orientation values between both UAVs in respect to the rear UAV body-fixed frame, in order to maintain the rear UAV over the desired relative position while orientated with respect to the desired relative orientation.

The full dynamical model of the configuration proposed is derived from the Lagrangian mechanics, modeling the payload as a 6 degree of freedom rigid body and the cables which attach the payload to the UAVs as mass-less rigid links. The cables are assumed to be always stretched. The controllers proposed are designed based on a linearization of these dynamics under some simplifying assumptions, e.g. neglecting the load torque. Since it is meant to control the rear UAV relative position and orientation with respect to its body-fixed frame, and assuming that both UAVs share the same dynamics, the dynamical system upon which it is meant to base the control design can be represented by:

$$\begin{aligned} m\dot{\boldsymbol{v}}_{rel} &= \mathbf{f}_F^{\mathcal{I}} - \mathbf{f}_R^{\mathcal{I}} \\ \dot{\boldsymbol{p}}_{rel} &= \boldsymbol{v}_{rel} \\ \mathbf{z} &= \mathbf{C}\boldsymbol{p}_{rel} \end{aligned} \tag{21}$$

where $\boldsymbol{v}_{rel} = \boldsymbol{v}_F - \boldsymbol{v}_R$, $\boldsymbol{p}_{rel} = \boldsymbol{p}_F - \boldsymbol{p}_R$, and $\mathbf{C}$ is the output matrix. Since $\mathbf{f}_F^{\mathcal{I}}$ is the front UAV actuation force vector, $\mathbf{f}_F^{\mathcal{I}}$ is assumed as an external disturbance. The relative attitude angles are depicted as $\boldsymbol{\eta}_{rel}$.

An external control loop is designed taking into consideration that $\boldsymbol{p}_{rel}$, $\boldsymbol{v}_{rel}$, and $\boldsymbol{\eta}_{rel}$, can be measured resorting to the motion tracking system. The external control loop expects a reference relative position and orientation, and combines these references with the sensors measurements in order to obtain the desired roll, pitch, angular velocity around the yaw axis and vertical velocity, which are the attitude inner loop set of inputs. The inner attitude control loop is responsible for prescribing these inputs into individual rotors velocities. The control system architecture is depicted in Fig. 1.

Since the relative position control design is based on the rear UAV body-fixed frame, the relative position tracking errors with respect to the NED frame are given by:

$$\boldsymbol{e}_p = \boldsymbol{r}_p - \boldsymbol{R}_{\mathcal{I}}^{\mathcal{B}}\boldsymbol{p}_{rel} \tag{22}$$

where $\boldsymbol{r}_p = (x_d, y_d, z_d)^T$ is the desired relative position reference vector between both UAVs in respect to the rear UAV body-fixed frame, and $\boldsymbol{R}_{\mathcal{I}}^{\mathcal{B}}$ is the rotation matrix that describes the rotation of the NED frame into the rear UAV body-fixed frame.

Therefore, the inner control loop input vector is computed as follows:

$$\begin{bmatrix} u_x \\ u_y \\ u_z \end{bmatrix} = \begin{bmatrix} K_x & 0 & 0 \\ 0 & K_y & 0 \\ 0 & 0 & K_z \end{bmatrix} \boldsymbol{e}_p - \mathbf{K}_{xyz} \begin{bmatrix} \boldsymbol{v}_{rel} \\ \boldsymbol{\eta}_{rel} \\ \boldsymbol{\zeta} \end{bmatrix} \tag{23}$$

where K_x, K_y, and K_z are the position optimal gains, and $\mathbf{K}_{xyz}$ is the optimal gain matrix suppressing the gains regarding the position states.

Resorting to relative position in respect to the NED frame, the relative yaw orientation from the rear to the front UAV can be computed as:

$$\psi_r = \psi_R + tan^{-1}\left(\frac{y_F - y_R}{x_F - x_R}\right) \tag{24}$$

Therefore, the orientation input control vector for the rear UAV is presented in (25).

$$u_\psi = K_\psi(r_\psi - \psi_r) \tag{25}$$

6. Estimation

Vertical and ground velocities are estimated based upon position measurements, resorting to complementary filters, as detailed in [19].

6.1. Relative position and orientation filter (frontal camera)

In order to estimate the relative position, velocity and orientation between the two UAVs, the filter architecture proposed in [20] was exploited. The filter presents a Visual-Aided landmark positioning system together with an IMU using complementary filters. Using a landmark tracking system using color feature recognition based on the Mahalanobis distance, position and attitude relative to a target are retrieved via the algebraic Robust solution to the Perspective-n-Point (RPnP) [21]. The measurements obtained are then fused with the optical flow available on-board.

The following state-space representation describes the position kinematics using the body velocity as input:

$$\begin{aligned} \begin{bmatrix} \boldsymbol{x} \\ \boldsymbol{b}_v \end{bmatrix}_{k+1} = \begin{bmatrix} \mathbf{I} & -\Delta\boldsymbol{R}_k \\ \mathbf{0} & \mathbf{I} \end{bmatrix} \begin{bmatrix} \boldsymbol{x} \\ \boldsymbol{b}_v \end{bmatrix}_k + \begin{bmatrix} \Delta\boldsymbol{R}_k \\ \mathbf{0} \end{bmatrix} \boldsymbol{v}_k + \\ \begin{bmatrix} \Delta\boldsymbol{R}_k & \mathbf{0} \\ \mathbf{0} & \mathbf{I} \end{bmatrix} \begin{bmatrix} \boldsymbol{n}_p \\ \boldsymbol{n}_b \end{bmatrix}_k \end{aligned} \tag{26}$$

where $\boldsymbol{x}$ is the position in the inertial frame, $\boldsymbol{v}$ is the velocity in fixed-body frame coordinates, $\boldsymbol{R}$ denotes the rotational matrix from the body-fixed frame $\{\mathcal{B}\}$ to the inertial frame $\{\mathcal{I}\}$ placed at the landmarks plane, $\boldsymbol{b}_v$ represents the velocity bias that accounts for the velocity of the moving target model uncertainties and errors in the optical flow estimate, and $\boldsymbol{n}_p$ and $\boldsymbol{n}_b$ denote zero-mean Gaussian white-noise that accounts for disturbances in the position and in the velocity bias, respectively.

The position observer, with uniformly asymptotic stability proof [20], is given by the following nonlinear feedback system:

$$\begin{aligned} \begin{bmatrix} \hat{\boldsymbol{x}} \\ \hat{\boldsymbol{b}}_v \end{bmatrix}_{k+1} = \begin{bmatrix} \mathbf{I} & -\Delta\boldsymbol{R}_k \\ \mathbf{0} & \mathbf{I} \end{bmatrix} \begin{bmatrix} \hat{\boldsymbol{x}} \\ \hat{\boldsymbol{b}}_v \end{bmatrix}_k + \begin{bmatrix} \Delta\boldsymbol{R}_k \\ \mathbf{0} \end{bmatrix} \boldsymbol{v}_k + \\ \begin{bmatrix} \boldsymbol{R}_k(\boldsymbol{K}_{1\boldsymbol{x}} - \mathbf{I}) + \boldsymbol{R}_{k-1} \\ \boldsymbol{K}_{2\boldsymbol{b}_v} \end{bmatrix} \boldsymbol{R}_{k-1}^T (\boldsymbol{x}_k - \hat{\boldsymbol{x}}_k) \end{aligned} \tag{27}$$

where $\boldsymbol{K}_{1\boldsymbol{x}}$, and $\boldsymbol{K}_{2\boldsymbol{b}_v}$ are the Kalman gains computed for the system presented in (26) with $\boldsymbol{R}_k = \mathbf{I}$, which are proved to be the optimal gains for the filter (27). The relative body velocity $\boldsymbol{v}_{rel}$ is then estimated as:

$$\hat{\boldsymbol{v}}_{rel\,k} = \boldsymbol{v}_k - \hat{\boldsymbol{b}}_{v\,k} \tag{28}$$

For the purpose of not losing the target, one requirement is that the rear UAV should always try to focus the center of mass of the front UAV. With that in view, the control reference in yaw for the rear UAV has to be given in terms of the relative position as:

Fig. 4. UAV - Parrot Ar.Drone 2.0 quadrotor.

$$r_{\psi} = tan^{-1}\left(\frac{\hat{y}_{rel}}{\hat{x}_{rel}}\right) \tag{29}$$

where $\hat{y}_{rel}$ and $\hat{x}_{rel}$ are the relative position $\hat{\boldsymbol{x}}$ in (27).

The measurement of the position filter presented in (27) is given by a landmark target consisting of 6 markers. The landmarks are placed in the same plane, and a YCbCr color segmentation via Mahalanobis distance is used for the segmentation of the markers from the background. After segmenting the markers, the respective centroids are computed and, the RPnP technique is used, providing the position and orientation of the camera relative to the landmark's target plane. Only the position in X and Y-axis, and the yaw angle, from the tracking system, is exploited as a measurement for filtering.

7. Experimental setup and results

This section describes the UAV under study, the respective physical model and the tools used in order to implement the proposed solutions. This information is mandatory for a better understanding of the UAV to be used in regard to its specifications and limitations.

7.1. UAV

The model used for this study is a Parrot Ar.Drone 2.0. An image of the model is depicted in Fig. 4. The Parrot Ar.Drone 2.0 is equipped with four "inrunner" brush-less motors of 14.5 W and a maximum rotation speed of 28500 rpm, each controlled by a ATMEGA 8-bit micro-controller. The motors are controlled through PWM (Pulse Width Modulation) commands in a range from 0% to 100%. Two rotors rotate clockwise, while other two rotors rotate counter-clockwise. The UAVs are equipped with an ARM Cortex A8 1 GHz 32-bit processor with 800 MHz TMS320DMC64X and a DDR2 1 GB at 200 MHz RAM, operating under Linux 2.6.32 OS.

This UAV is also endowed with an inboard IMU, a 720p 30 fps HD frontal camera capable of HD video recording, and a QVGA 60 fps vertical camera for ground velocities measurements resorting to optical flow techniques.

The inboard IMU is composed by a 3-axis gyroscope with an accuracy of 2.000 degree/s, a 3-axis accelerometer with an accuracy of $\pm$50 mG, a 3-axis magnetometer with an accuracy of 6 degrees. This IMU allows the measurement of the height, attitude angles, accelerations, ground velocities, and angular velocities. Moreover, a pressure sensor with an accuracy of $\pm$10 Pa, an ultrasonic transmitter, and an ultrasonic receiver are also present on-board.

In Fig. 5, the experimental setup is shown. The Parrot Ar.Drone 2.0 is controlled via WIFI in a range of 50 m, having its own network defined as an access point. Parrot also provides a dedicated free app for the control of the quadrotor, live video streaming, making films, and taking pictures.

In order to implement the control systems designed for the two UAVs, the AR Drone Simulink Development-Kit V1.1 (DevKit) provided in [22] is used. This Devkit provides Simulink based models for the WIFI communication between both UAVs and a terminal, for instance, a personal computer. Here the control system is implemented in external mode. These Simulink models allow sending a combination of attitude (desired angles) and vertical speed commands as input control commands to the Ar.Drone embedded attitude inner control loop, and reading the states available upon the state reconstruction from the sensor data also built in the embedded electronics simultaneously. The state reconstruction provides estimations of the altitude, attitude angles, ground velocities.

For the experimental implementation of the control systems proposed, it is required to work in discrete time. The selected sample time for the controllers and filters is 0.065 s, taking into consideration the slowest sensor built in the UAV, namely, the ultrasound which operates at a minimum sample time of 0.04 s. Therefore, the Qualisys system used as ground truth to the relative position and orientation is also set to work at a sample time of 0.065 s.

In order to reduce the ultrasound signal interferences between both UAVs, resulting in conflicts on the altitude estimation of both subsystems, one of the UAVs was set to operate at a different signal frequency. The reference distance along the longitudinal direction for the relative position was set to 3.5 m.

The rear UAV, which is responsible for regulating the relative position, the controller was designed aiming a faster response than the front UAV, in order to compensate more efficiently the delay present in the system.

A video showing the collaborative load transportation reported in [19] can be found in https://youtu.be/QlUf5pb1f1w, but using a motion capture system. In this work, the motion capture system is only used for ground truth purposes.

7.2. Step analysis

The LQR controller gains for the front and rear UAV were calculated using the weighting matrices presented in Table 1 and Table 2, and are presented in Table 3 and Table 4.

In Fig. 6 the experimental results regarding the consequent unit step responses are presented. Here, the unit step responses for the XYZ directions regarding the front UAV present a settling time (5%) is at 5.4 s, 5.6 s, and 8.9 s, respectively. The maximum overshoot is 3.8 cm, 3.6 cm, and 0 cm for the XYZ directions. The relative position between both UAVs along the XYZ directions settles at 6 s, 6 s, and 8 s, respectively. The maximum relative position errors between both UAVs along the XYZ directions are 35 cm, 22 cm, 43 cm, respectively. These errors are relatively high during the transient response but remain much lower when steady state is achieved after around 12 s. The fact that a collaborative approach is pursued, where the commands or references by the human operator are not known in advance, leads to errors that are relatively higher during the transient response but they decrease when the steady state is achieved. The severity of those errors is directly related to the aggressiveness of the human commands. The simulated step responses provide reasonable good approximations compared to the real response, in the sense that they converge to the reference with stability. The dynamics of these responses vary because of several reasons like non-perfect cross coupling terms, properties mismatch, simulated and real noise, non modeled nonlinearities like turbulence resulting from both drones working close together as well as payload dynamics. These discrepancies are more evident in Fig. 6(c) which is the one that corresponds to the direction of the movement.

The control performance regarding the control of the relative position is presented in Table 5. For the evaluation of the performance is analyzed the settling time of the relative position regarding a 5 cm criteria mentioned before, maximum relative error and the root mean square error.

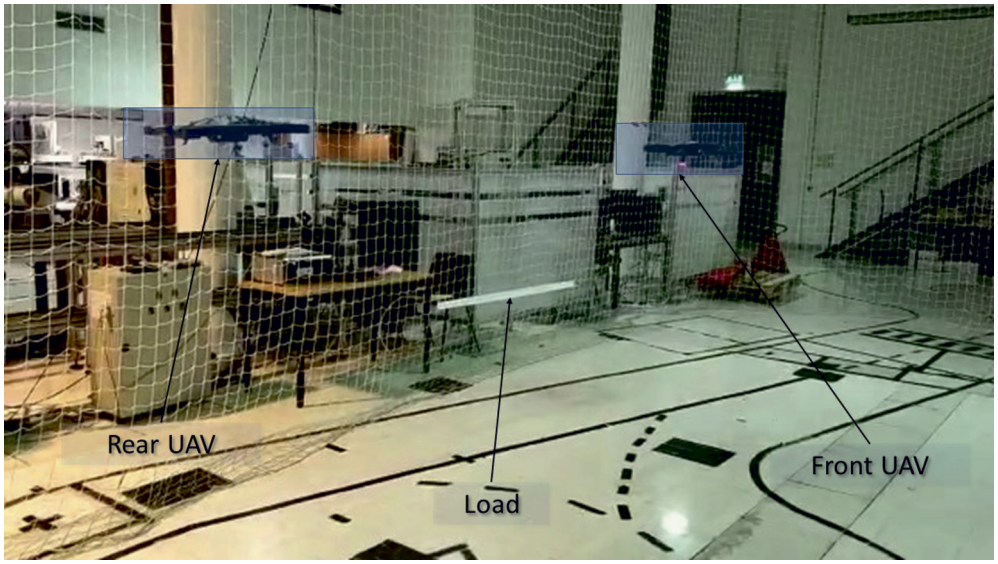

Fig. 5. Experimental setup.

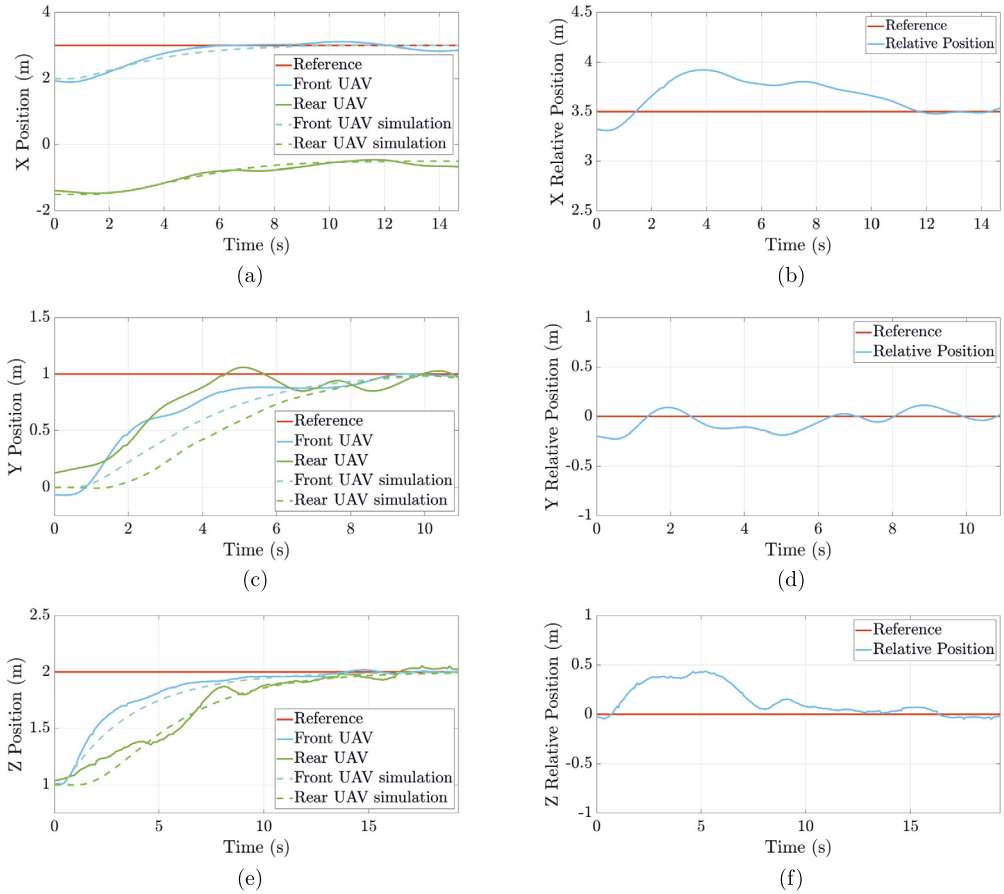

Fig. 6. Step-analysis experimental results. From left to right, top to bottom: (a) X Position, (b) X Relative Position, (c) Y Position, (d) Y Relative Position, (e) Z Position, (f) Z Relative Position. (For interpretation of the colors in the figures, the reader is referred to the web version of this article.)

Table 1
Front UAV LQR weighting matrices.

	X Position	Y Position	Z Position
Q	*diag*(3, 1, 1, 0)	*diag*(3, 1, 1, 0)	*diag*(3, 1)
R	520	220	25

Table 2
Rear UAV LQR weighting matrices.

	X Position	Y Position	Z Position
Q	*diag*(3, 1, 1, 0)	*diag*(3, 1, 1, 0)	*diag*(3, 1)
R	430	180	20

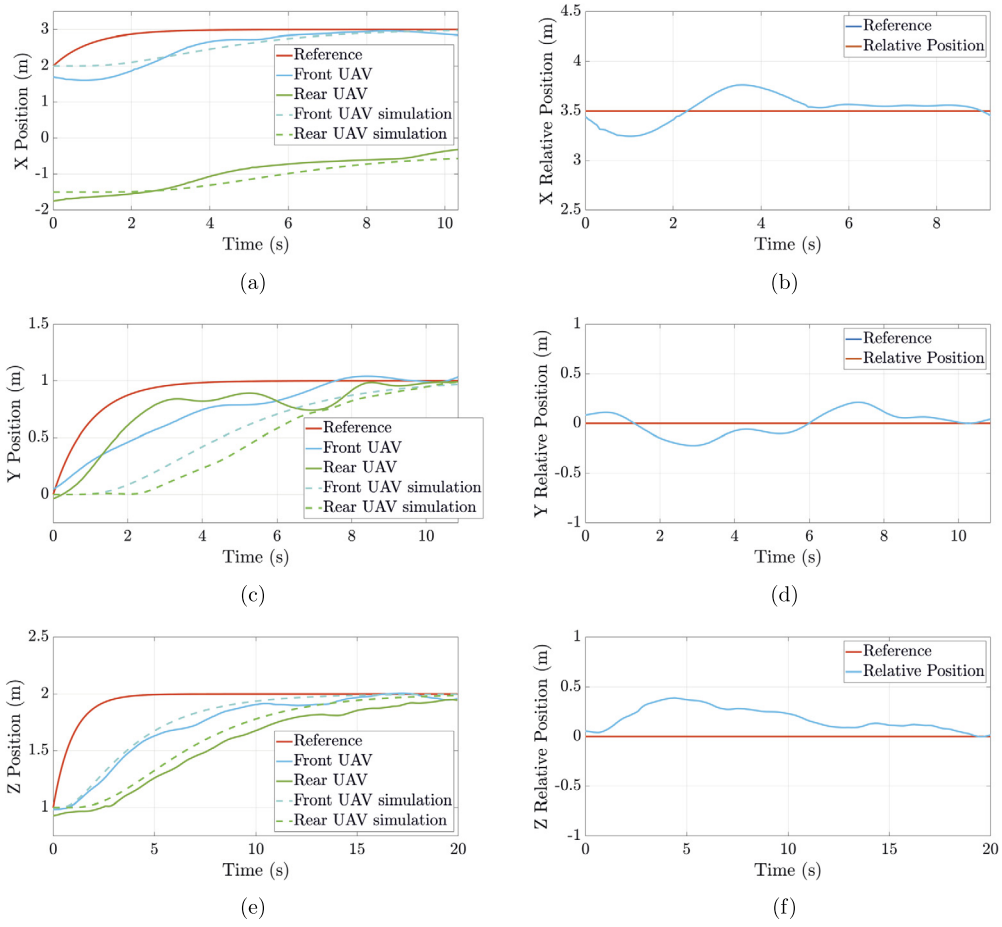

Fig. 7. Intermediary filter experimental results. From left to right, top to bottom: (a) X Position, (b) X Relative Position, (c) Y Position, (d) Y Relative Position, (e) Z Position, (f) Z Relative Position.

Table 3
Front UAV experimental LQR gains.

	Gains
X Position	$\begin{bmatrix} -0.0753 & -0.0978 & 0.2009 & 0.0480 \end{bmatrix}$
Y Position	$\begin{bmatrix} 0.1156 & 0.2323 & 0.0794 & 0.0156 \end{bmatrix}$
Z Position	$\begin{bmatrix} 0.3425 & 0.0688 \end{bmatrix}$

Table 4
Rear UAV experimental LQR gains.

	Gains
X Position	$\begin{bmatrix} 0.0828 & 0.1063 & -0.2183 & -0.0519 \end{bmatrix}$
Y Position	$\begin{bmatrix} -0.1277 & -0.2526 & -0.0870 & -0.0169 \end{bmatrix}$
Z Position	$\begin{bmatrix} -0.3823 & -0.0781 \end{bmatrix}$

Table 5
Step analysis - rear UAV experimental performance.

	Settling time (5%)	Max. error	RMS error
X Position	11 s	42.2 cm	23.29 cm
Y Position	6 s	22 cm	10.45 cm
Z Position	8 s	43 cm	20.25 cm

7.3. Intermediary filters

For the front UAV, the LQR controller gains, computed considering the state **Q** and input **R** weighting matrices presented in Table 1, are presented in Table 3. For the rear UAV, the LQR controller gains are computed considering the state and input weighting matrices presented in Table 2, and are shown in Table 4. The experimental results concerning the design and implementation of the low pass intermediary filters and complementary filters are presented in Fig. 7. Here, the results in the XYZ directions regarding the front UAV present a settling time (5%) is at 8.0 s, 10.5 s, and 10.0 s, respectively. The maximum overshoot is 0 cm, 4.1 cm, and 0.7 cm for the XYZ directions. The control system performance concerning the relative position is evaluated resorting to a 5 cm settling time criteria, maximum relative error and the root mean square error, which results are presented in Table 6. The settling time criteria assume that the relative position error settles for values less than 5 cm.

For the X Position the prediction failed, where is noted a significant reduction to less than half of the settling time concerning the relative position error. This reduction can be justified by the demand for a response too aggressive for the control system designed for the rear UAV. Nevertheless, the implementation of the low pass filter restricted the frequency bandwidth of the system, resulting in lower frequency responses less demanding for the rear UAV to track, since the rear UAV actuators and control system present limited frequency bandwidth. This fact may also explain the slightly unexpected increase of the root mean square error, alongside the maximum relative error that remained equal.

7.4. Position and orientation filters results

In this section, is presented the experimental results concerning the implementation of the position and orientation filter presented

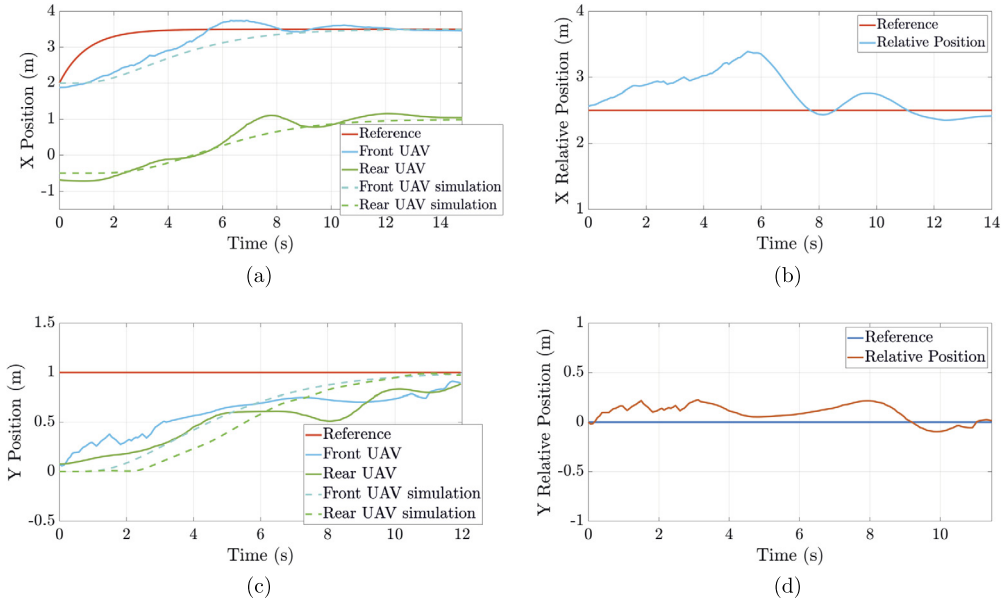

Fig. 8. Position and orientation filter experimental results. From left to right, top to bottom: (a) X Position, (b) X Relative Position, (c) Y Position, (d) Y Relative Position.

Table 6
Intermediary filters - rear UAV experimental performance.

	Settling time (5%)	Max. error	RMS error
X Position	5 s	27.0 cm	14.19 cm
Y Position	8 s	22.0 cm	11.70 cm
Z Position	10 s	38.8 cm	19.39 cm

Table 7
Position and orientation filter - rear UAV experimental performance.

	Settling time (5%)	Maximum error	Root mean square error
X Position	10.6 s	88.8 cm	34.78 cm
Y Position	9.0 s	22.6 cm	12.54 cm

previously. Here, the relative position and orientation are estimated resorting to rear UAV front camera. Therefore, the motion tracking system only is used to provide ground truth measurements, since all the estimation process is being done resorting only on-board sensors installed on the UAV. The position filter in use is designed only for estimations along the X and Y directions, thus only is presented the results regarding steps in these directions. The height is set to be constant during the experimental flights, being controlled resorting to altimeter measurements.

The front UAV integrates its ground velocities corrected by its yaw angle to estimate its position. Thus, since it is controlled the estimated position based only on optical flow measurements where noise is present, the position estimation gradually starts to drift.

Due to the UAV limitations in terms of payload carrying capacity, the target to be placed on the front UAV upon which is meant to estimate the relative position and orientation has to be relatively small. Thus, the camera was only able to take measurements on the target until a maximum relative distance of 4 m. However, since it meant to measure the movement of the front UAV, an abrupt maneuver may lead to the domain where the camera is not able to take measurements of the target. Therefore, the desired relative distance along the longitudinal direction X was set to 2.5 m instead of 3.5 m. This change leads to more accentuate altimeter inferences and air-flow cross disturbances, resulting in poor performance of the control system. The altimeter inferences induce in poor measurements of the height directly influencing the optical flow measurements which resort to the estimation of the height.

For the front UAV, the LQR controller gains, computed considering the state **Q** and input **R** weighting matrices presented in Table 1, are presented in Table 3. For the rear UAV, the LQR controller gains are computed considering the state and input weighting matrices presented in Table 2, and are shown in Table 4. The experimental results concerning the design and implementation of the intermediary filters and position filter are presented in Fig. 8. The control system performance is evaluated resorting to a 5 cm settling time criteria, maximum relative error and the root mean square error, which results are presented in Table 7. The settling time criteria assume that the relative position error settles for values less than 5 cm.

The results presented denote very similar properties to the results presented in Fig. 7. Along the Y direction, the front UAV position settles at 10.2 s presenting an increase of 2.2 s, and the rear UAV settles the relative position at 9.0 s presenting a maximum relative position error of 22.6 cm and an increase of the root mean square error to 12.54 cm. Along the X direction, the front UAV position settles at 10.6 s presenting an increase of 2.2 s, and the rear UAV settles the relative position at 7.0 s presenting a maximum relative position error of 88.8 cm and an increase of the root mean square error to 34.78 cm.

The deterioration of the control performance is due the fact that the control system is now only dependent on on-board sensors installed in the quadrotor, and the rectangular shape placed at the top of the front UAV. Since the target developed for this application presents a rectangular shape and is placed aligned with the front UAV referential frame, the inertia of the quadrotor gets compromised. The target has almost no thickness, presenting almost null variations on the inertial regarding the X direction which is directly related to the roll angles that governs the movement along the Y direction. However, the rectangular shape of the target induces a significant increase of the inertial concerning the Y direction, resulting in a more accentuated poor control system performance when compared to the result presented in Fig. 7, since the pitch moment to be generated by the rotors has to be significantly higher. Nevertheless, the results presented in Fig. 8 still prove the feasibility of the control system designed to perform the task, where the relative position converges presenting no steady-state error and satisfactory performances having in mind the assumptions done during the controllers' design phase.

The simplifying assumption to ignore the pitch and roll degrees of freedom on the load is considered. The impact on the selected control structure is revealed, for instance, in the Y direction as depicted in pictures 6(c), 7(c), and 8(c) or in the roll or pitch angles of the load (not sensed in this phase of the work). However, if more than two UAVs were used, these issues would not be present. The general analysis is out of the scope of this paper and will be addressed in future work. From the experimental results observed, the coupling and the associated phenomena with the load were revealed but the dynamic behavior of the relevant state variables met the specifications set forth.

8. Conclusion

This paper presented a methodology for collaborative load transportation by two quadrotors, given the state variables estimates, based on measurements from motion sensors installed on-board. The control and estimation solutions were required to ensure the stability of the system while guarantying a null steady-state position and estimation errors. The vertical velocity has to be estimated since there is no sensor usually on-board the quadrotors capable of providing this measurement directly.

Further, in order to turn the system independent of a motion tracking system to provide estimates of the relative position between the multiple UAVs, the UAVs, front camera is used in order to provide these estimates. Therefore, the relative velocity between the UAVs can be estimated upon these measurements.

The proposed solutions are presented based on linear control and estimation methods. These solutions include classical and optimal control and estimation theory. The controllers and estimators resort to linear and optimal control techniques, as LQRs and Kalman filters, respectively.

The proposed control system is validated both in simulation and experimentally, resorting to a commercially available quadrotor equipped with an IMU, an ultrasound height, vertical, and frontal cameras, among other sensors. The simulation environment models the noise present in the measurements provided by the sensors, as Gaussian white-noise for the experimental implementation of the control system proposed. The observed results meeting the specifications and from the Front UAV operator point of view, the set of tests were satisfactory.

Declaration of competing interest

The authors declare that they have no known competing financial interests or personal relationships that could have appeared to influence the work reported in this paper.

Acknowledgements

This work is financed by national funds through FCT - Foundation for Science and Technology, I.P., through IDMEC, under LAETA, project UIDB/50022/2020 and project REPLACE (LISBOA-01-0145-FEDER-032107) from the Portuguese Foundation for Science and Technology (FCT).

References

[1] M. Hassanalian, A. Abdelkefi, Classifications, applications, and design challenges of drones: a review, Prog. Aerosp. Sci. (ISSN 0376-0421) 91 (2017) 99–131.
[2] Emanuele L. de Angelis, Fabrizio Giulietti, Goele Pipeleers, Two-time-scale control of a multirotor aircraft for suspended load transportation, Aerosp. Sci. Technol. 84 (2019) 193–203.
[3] Hae-In Lee, Dong-Wan Yoo, Byung-Yoon Lee, Gun-Hee Moon, Dong-Yeon Lee, Min-Jea Tahk, Hyo-Sang Shin, Parameter-robust linear quadratic Gaussian technique for multi-agent slung load transportation, Aerosp. Sci. Technol. 71 (2017) 119–127.
[4] Giuseppe Loianno, Vijay Kumar, Cooperative transportation using small quadrotors using monocular vision and inertial sensing, IEEE Robot. Autom. Lett. 3 (2) (2017) 680–687.
[5] Behzad Shirani, Majdeddin Najafi, Iman Izadi, Cooperative load transportation using multiple uavs, Aerosp. Sci. Technol. 84 (2019) 158–169.
[6] Ivan Maza, Konstantin Kondak, Markus Bernard, Aníbal Ollero, Multi-uav cooperation and control for load transportation and deployment, in: Selected Papers from the 2nd International Symposium on UAVs, Reno, Nevada, USA, June 8–10, 2009, Springer, 2009, pp. 417–449.
[7] Sandesh Thapa, He Bai, J.A. Acosta, Cooperative aerial load transport with force control, IFAC-PapersOnLine 51 (12) (2018) 38–43.
[8] Ngoc Anh Vu, Duy Khang Dang, Tuan Le Dinh, Electric propulsion system sizing methodology for an agriculture multicopter, Aerosp. Sci. Technol. 90 (2019) 314–326.
[9] Richard M. Murray, Trajectory generation for a towed cable system using differential flatness, in: IFAC World Congress, 1996, pp. 395–400.
[10] Sarah Tang, Vijay Kumar, Mixed integer quadratic program trajectory generation for a quadrotor with a cable-suspended payload, in: 2015 IEEE International Conference on Robotics and Automation (ICRA), IEEE, 2015, pp. 2216–2222.
[11] P. Outeiro, C. Cardeira, P. Oliveira, Adaptive/multi-model height control system of a quadrotor constant unknown load transportation, in: 2018 IEEE International Conference on Autonomous Robot Systems and Competitions (ICARSC), April 2018, pp. 65–70.
[12] Jonathan Fink, Nathan Michael, Soonkyum Kim, Vijay Kumar, Planning and control for cooperative manipulation and transportation with aerial robots, Int. J. Robot. Res. 30 (3) (2011) 324–334.
[13] Nathan Michael, Jonathan Fink, Vijay Kumar, Cooperative manipulation and transportation with aerial robots, Auton. Robots 30 (1) (2011) 73–86.
[14] K. Ogata, Modern Control Engineering, Instrumentation and Controls Series, Prentice Hall, ISBN 9780136156734, 2010.
[15] R. Mahony, V. Kumar, P. Corke, Multirotor aerial vehicles: modeling, estimation, and control of quadrotor, IEEE Robot. Autom. Mag. (ISSN 1070-9932) PP (99) (2012) 1.
[16] Taeyoung Lee, Melvin Leok, N. Harris McClamroch, Global Formulations of Lagrangian and Hamiltonian Dynamics on Manifolds, Springer, 2017.
[17] Taeyoung Lee, Geometric control of multiple quadrotor uavs transporting a cable-suspended rigid body, in: 53rd IEEE Conference on Decision and Control, IEEE, 2014, pp. 6155–6160.
[18] Brian D.O. Anderson, J.B. Pren, S.L. Dickerson, Linear Optimal Control, Prentice Hall, 1971.
[19] Tiago Bacelar, Carlos Cardeira, Paulo Oliveira, Cooperative load transportation with quadrotors, in: 2019 IEEE International Conference on Autonomous Robot Systems and Competitions (ICARSC), IEEE, 2019, pp. 1–6.
[20] João Madeiras, C. Cardeira, Paulo Oliveira, Complementary filter aided vision for attitude and position estimation: design, analysis and experimental validation, in: 21st IFAC Symposium on Automatic Control in Aerospace (ACA), 2019.
[21] S. Li, C. Xu, M. Xie, A robust o(n) solution to the perspective-n-point problem, IEEE Trans. Pattern Anal. Mach. Intell. (ISSN 0162-8828) 34 (7) (July 2012) 1444–1450.
[22] D.E. Sanabria, P.J. Mosterman, AR drone simulink development-kit v1.1, https://www.mathworks.com/matlabcentral/fileexchange/43719, November 2014.